A nonlinear controller based on saturation functions with variable parameters to stabilize an AUV

Eduardo Campos Mercado, Jesus Monoroy, Hugo Abundis, Ahmed Chemori, Vincent Creuze, Jorge Torres

International Journal of Naval Architecture and Ocean Engineering xxx (2018) 1–14

Contents lists available at ScienceDirect

International Journal of Naval Architecture and Ocean Engineering

journal homepage: http://www.journals.elsevier.com/international-journal-of-naval-architecture-and-ocean-engineering/

A nonlinear controller based on saturation functions with variable parameters to stabilize an AUV

E. Campos [a, *], J. Monroy [d], H. Abundis [a], A. Chemori [c], V. Creuze [c], J. Torres [b]

[a] CONACYT-Universidad del Istmo, Tehuantepec, Oaxaca, Mexico
[b] Automatic Control Department, CINVESTAV, CDMX, Mexico
[c] LIRMM, CNRS-Université de Montpellier 2, Montpellier, France
[d] Universidad Politecnica de Tulancingo, Hidalgo, Mexico

ARTICLE INFO

Article history:
Received 26 January 2017
Received in revised form
1 March 2018
Accepted 4 April 2018
Available online xxx

Keywords:
AUV
Nonlinear PD and PD+ controllers
Real-time experiments

ABSTRACT

This paper deals with a nonlinear controller based on saturation functions with variable parameters for set-point regulation and trajectory tracking control of an Autonomous Underwater Vehicle (AUV). In many cases, saturation functions with constant parameters are used to limit the input signals generated by a classical PD (Proportional-Derivative) controller to avoid damaging the actuators; however this abrupt bounded harms the performance of the controller. We, therefore, propose to replace the conventional saturation function, with constant parameters, by a saturation function with variable parameters to limit the signals of a PD controller, which is the base of the nonlinear PD with gravitational/buoyancy compensation and the nonlinear PD + controllers that we propose in this paper. Consequently, the mathematical model is obtained, considering the featuring operation of the underwater vehicle LIRMIA 2, to do the stability analysis of the closed-loop system with the proposed nonlinear controllers using the Lyapunov arguments. The experimental results show the performance of an AUV (LIRMIA 2) for the depth control problems in the case of set-point regulation and trajectory tracking control.

1. Introduction

Nowadays the increased interest in AUV is fueled by a wide variety of military and civil applications, among which we can highlight underwater inspection, surveillance, oil rigs monitoring, archaeological studies, to name a few. Outstanding technological progress in the performance, control and autonomous behavior makes the AUV's a powerful tool (for example (Stewart and Glegg, 2010; Quidu and Jaulin, 2012; Kleeman; Zhao and Liu, 2016)). However, the main challenge for this kind of vehicle lies in the implementation of the control strategy for doing different tasks given the nonlinear dynamics and the difficulty to identify its hydrodynamic parameters accurately. These topics still remain of interest within different research communities (see (Newman, 1977; Lamb, 1932; Fossen, 2011; Jung and Paik, 2017)).

Current literature contains various control strategies such as sliding mode control (Wallace and Bessa, 2008), adaptive control (Maalouf and Tamanaja, 2013), neuronal network control (Kawano and Ura, 2002) and nonlinear control (Sanahuja et al., 2009; Shang and Cong, 2009), that has been successfully applied to set-point regulation; as well as trajectory tracking control of Autonomous Underwater Vehicles. However, one of the most typical control strategies used in real applications is the PD controller with different approaches, although this controller does not have a good performance when the system parameters change. In previous work, we obtained successfully results using the control strategy based on saturation functions with constant parameters (Campos and Torres, 2012). Consequently, we propose to modify the classical PD controller with the implementation of a saturation function with variable parameters, thus achieving robustness in the closed-loop system.

The main contributions of this paper are summarized as follows:

- We present nonlinear controllers with variable gains for set-point regulation and trajectory tracking control of an Autonomous Underwater Vehicle.
- We have done the stability analysis of the closed-loop system using the Lyapunov technique.

* Corresponding author.
E-mail address: ecampos@conacyt.mx (E. Campos).
Peer review under responsibility of Society of Naval Architects of Korea.

https://doi.org/10.1016/j.ijnaoe.2018.04.002

- We present the real-time experimental results of the closed-loop system.

Experiments have been done for trajectory tracking control in a nominal case and when the weight of the vehicle is changed, to show the robustness of the nonlinear PD controller.

This paper is organized as follows: In section II, we briefly describe the dynamic model of the mini-submarine *LIRMIA*2. The control strategy is presented in section III. The experiments using a linear and nonlinear PD controllers for trajectory tracking control are presented and discussed in section IV. Finally, some concluding remarks and future works are given in section V.

2. Dynamic modeling of the vehicle

We have designed and built the *LIRMIA*2 AUV, which is depicted in Fig. 1 and its main features are described in Table 1. The center O_b of its body-fixed frame corresponds to the center of gravity of the vehicle; and its axes are aligned with the main axes of symmetry of the vehicle. The motion in the horizontal plane is referred as *surge* (along the x_b axis) and *sway* (along the y_b axis), while *heave* represents the vertical motion (along the z_b axis). Roll, pitch, and yaw, denoted by (ϕ,θ,ψ), are the Euler angles describing the orientation of the vehicle's body-fixed frame with respect to the earth-fixed frame (O_I,x_I,y_I,z_I), while (x,y,z) denote the coordinates of the center of the body-fixed frame in the earth-fixed frame. The propulsion system consists of eight thrusters, as illustrated in Fig. 2. Some thrusters are connected to the same driver, thus we can assume that $f_1 = f_2, f_3 = f_4, f_5 = f_6$ and $f_7 = f_8$, that is why the roll motion is unactuated. The rotational motion of this vehicle, yaw movement is performed through differential speed control of thrusters 3, 4, 5 and 6. Pitch motion is obtained similarly using thrusters 1, 2, 7, and 8. The translational motion through the z axis is regulated by decreasing or increasing the combined speed of thrusters 1, 2, 7, and 8. Similarly, the translational motions along the x_b and y_b axes are obtained by using thrusters 3, 4, 5, 6 and by controlling the yaw angle.

The dynamics of the vehicle, expressed in the body-fixed frame, can be written in compact matrix form as (Fossen, 1999):

$$M\dot{\nu} + C(\nu)\nu + D(\nu)\nu + g(\eta) = \tau + w_e \tag{1}$$

$$\dot{\eta} = J(\eta)\nu \tag{2}$$

where $M \in \mathbb{R}^{6\times6}$ is the inertia matrix, $C(\nu) \in \mathbb{R}^{6\times6}$ defines the Coriolis-centripetal matrix, $D(\nu) \in \mathbb{R}^{6\times6}$ represents the hydrodynamic damping matrix, $g(\eta) \in \mathbb{R}^{6\times1}$ describes the vector of gravitational/buoyancy forces and moments, $\tau = (\tau_1,\tau_2)^T = ((\tau_X,\tau_Y,\tau_Z),(\tau_K,\tau_M,\tau_N))^T \in \mathbb{R}^{6\times1}$ defines the vector of control inputs (forces and moments); $w_e \in \mathbb{R}^{6\times1}$ defines the vector of disturbances; $\nu = (\nu_1,\nu_2)^T = ((u,v,w),(p,q,r))^T \in \mathbb{R}^{6\times1}$ denotes the linear and angular velocity vector in the body-fixed frame; $\eta = (\eta_1,\eta_2)^T = ((x,y,z),(\phi,\theta,\psi))^T \in \mathbb{R}^{6\times1}$ is the position and attitude vector decomposed in the earth-fixed frame, and $J(\eta) \in \mathbb{R}^{6\times6}$ is the transformation matrix mapping from body frame to earth-fixed frame, for more details, consult (Fossen, 1999; Goldstein et al., 1983; Marsden, 1974).

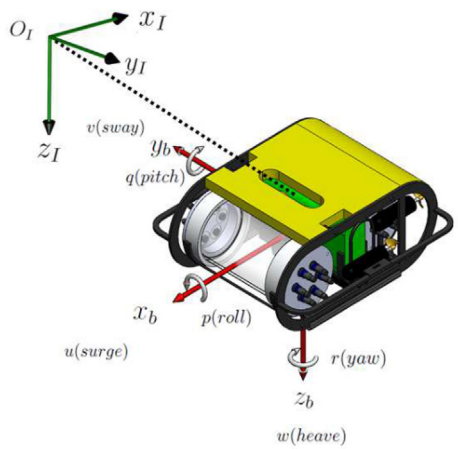

Fig. 1. The LIRMIA 2 vehicle, with a body-fixed frame (O_b,x_b,y_b,z_b), and an earth-fixed frame (O_I,x_I,y_I,z_I).

Table 1
The main features of the *LIRMIA*2 vehicle.

Mass	18.9 kg
Floatability	5N
Dimensions	40 cm (l) x 36 cm (w) x 25 cm (h)
Maximal depth	50 m
Thrusters	8 CD motor with propeller cont. bollard thrust = 0.8 kgf each with Fahrregler Rookie 20 WP drivers
Power	12 V - 500 W
Attitude sensor	UM6-LT Orientation Sensor
Camera	Webcam Logitech 9000 pro −30−fps
Depth sensor	Pressure Sensor Breakout MS5803-05BA
Sampling period	0.00236s
Embedded computer	FIT-PC2-Intel Atom Z550 2 GHz, 1 GB RAM, WiFi Windows XP Professional-32 bits Microsoft Visual C++ 2010

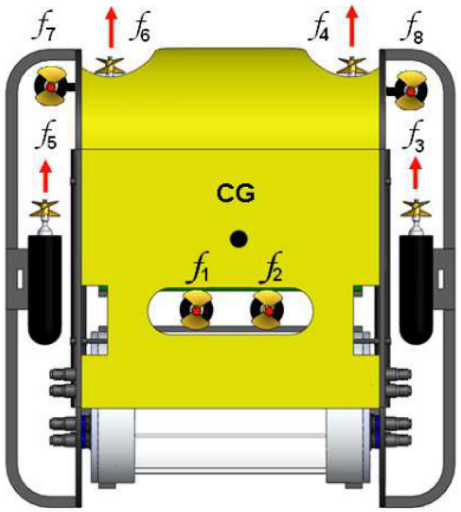

Fig. 2. CAD view of the robot with forces f_i, $i = 1..8$ generated by the eight thrusters of the vehicle. The position of the center of gravity is CG.

2.1. Inertia and Coriolis-centripetal matrices

The inertia matrix M is the sum of the rigid-body inertia M_{RB} and the inertia of the added mass M_A, as follows:

$$M = M_{RB} + M_A \tag{3}$$

In our case, we assume that the vehicle is moving at slow speeds; hence, the M matrix can be approximated by:

Please cite this article in press as: Campos, E., et al., A nonlinear controller based on saturation functions with variable parameters to stabilize an AUV, International Journal of Naval Architecture and Ocean Engineering (2018), https://doi.org/10.1016/j.ijnaoe.2018.04.002

$$M = diag\{m + X_{\dot{u}}, m + Y_{\dot{v}}, m + Z_{\dot{w}}, I_{xx} + K_{\dot{p}}, I_{yy} + M_{\dot{q}}, I_{zz} + N_{\dot{r}}\} \quad (4)$$

where m is the mass of the vehicle, I_{xx}, I_{yy}, I_{zz} are the moments of inertia of the rigid-body which are estimated by using the CAD design of the *LIRMIA*2 vehicle. Then, the obtained values are:

$$M_{RB} = diag\{21, 21, 21, 0.23, 0.42, 0.39\} \quad (5)$$

and $X_{\dot{u}}, Y_{\dot{v}}, Z_{\dot{w}}, K_{\dot{p}}, M_{\dot{q}}, N_{\dot{r}}$ represent hydrodynamic added mass estimated by using MCC (Marine Craft Characteristics; this freeware was created by ENSTA Bretagne and the link to download is cited in the following work (Yang et al., 2015)). The matrix of the added mass can be expressed as:

$$M_A = diag\{17.52, 23.18, 40.4, 0.25, 0.44, 0.41\} \quad (6)$$

Now, knowing the matrices M_{RB}, M_A and assuming that the center of gravity of the vehicle is in the origin of the body-fixed frame we can obtain the matrix $C(\nu)$ as is shown in (Fossen, 2002). Therefor, the Coriolis-centripetal matrix is described by the following equation:

$$C(\nu) = C_{RB}(\nu) + C_A(\nu) \quad (7)$$

with

$$C_{RB}(\nu) = \begin{bmatrix} 0 & -mr & mq & 0 & 0 & 0 \\ mr & 0 & -mp & 0 & 0 & 0 \\ -mq & mp & 0 & 0 & 0 & 0 \\ 0 & 0 & 0 & 0 & I_{zz}r & -I_{yy}q \\ 0 & 0 & 0 & -I_{zz}r & 0 & I_{xx}p \\ 0 & 0 & 0 & I_{yy}q & -I_{xx}p & 0 \end{bmatrix} \quad (8)$$

and

$$C_A(\nu) = \begin{bmatrix} 0 & 0 & 0 & 0 & -Z_{\dot{w}}w & Y_{\dot{v}}v \\ 0 & 0 & 0 & Z_{\dot{w}}w & 0 & -X_{\dot{u}}u \\ 0 & 0 & 0 & -Y_{\dot{v}}v & X_{\dot{u}}u & 0 \\ 0 & -Z_{\dot{w}}w & Y_{\dot{v}}v & 0 & -N_{\dot{r}}r & M_{\dot{q}}q \\ Z_{\dot{w}}w & 0 & -X_{\dot{u}}u & N_{\dot{r}}r & 0 & -K_{\dot{p}}p \\ -Y_{\dot{v}}v & X_{\dot{u}}u & 0 & -M_{\dot{q}}q & K_{\dot{p}}p & 0 \end{bmatrix} \quad (9)$$

Notice that the calculation errors of our added mass results can be considered as uncertainties in the parameter of the mathematical model.

2.2. Damping matrix

Concerning the hydrodynamic damping, we consider the damping model for low-speed underwater vehicles. Thus we have:

$$D(\nu) = diag\{X_u, Y_v, Z_w, K_p, M_q, N_r\} \quad (10)$$

The damping parameters of the vehicle that are included in the damping matrix have are experimental obtained by applying the following procedure. First, the buoyancy of the AUV is adjusted to exactly compensate for the weight, so that the buoyancy is neutral. Then, a known force is applied to the AUV along the z axis. This force is produced by the thrusters and it is known due to a previous calibration. As the vehicle submerses, the value of z is recorded (by the depth sensor). Then, the speed along z is computed. After few seconds, the AUV reaches a steady state limit speed. The value of Z_w, the damping parameter along z, is approximated by: $Z_w \simeq f_z / w_{lim}$, where f_z is the force exerted by the thrusters along z, and w_{lim} is the linear speed of the AUV along z. The estimated value of Z_w is 75.4 $N.s.m^{-1}$.

To compute the parameter Y_v, the cross sectional area of the vehicle and the shape of the body are quite the same in the z direction and in the y direction. Consequently, we consider that Y_v is roughly equal to Z_w. The value of X_u is computed by measuring the time needed by the AUV to run a known horizontal distance in a pool, with a known horizontal thrust. Then, the speed is computed and the damping parameter is estimated. The estimated value of X_u is 21.3 $N.s.m^{-1}$. Regarding the rotational damping parameter, we applied a known torque along z axis with the thrusters and we recorded the rate of turn measured by the gyrometer (along z axis) of the embedded IMU. Once the rate of turn reaches its steady state value r_{lim}, the rotational damping parameter N_r is approximated by: $N_r \simeq \gamma_z / r_{lim}$, where γ_z is the applied torque.

The estimated value of N_r is 1.6 $N.m.s.rad^{-1}$. The symmetry of the *LIRMIA*2 vehicle allows us to consider that M_q is roughly equal to N_r. The value of K_p (along x axis) has not been experimentally estimated as this would require making the center of gravity coincide with the center of buoyancy. This is long and useless, since in our case the roll is naturally stable and is not controlled. According to the previous values and the geometry of the vehicle, we have considered that $K_p \simeq 0.95$ $N.m.s.rad^{-1}$. Please note that we have assumed that the speed of the vehicle is sufficiently low to consider only the skin friction effects. Thus, we only estimate the linear damping. If the speed increase, then quadratic damping would be taken into account and quadratic damping parameters should be computed using the same method by replacing each speed by its squared value. Given that the vehicle is moving slow, non diagonal terms of the damping matrix are neglected and only linear damping parameters were estimated for this prototype:

$$D(\nu) = diag\{21.3, 70, 75.4, 0.95, 1.8, 1.6\} \quad (11)$$

in $\left(\frac{N.s}{m}\right)$ (first three) and in $\left(\frac{N.s}{rad}\right)$ (last three).

2.3. Gravity/Buoyancy forces and torques

According to Archimedes' principle, the buoyancy force f_B exerted at the center of the buoyancy and acts in the opposite direction of vehicle weight f_W. This leads to:

$$f_B = -\begin{bmatrix} 0 \\ 0 \\ \rho g \nabla \end{bmatrix} f_W = \begin{bmatrix} 0 \\ 0 \\ mg \end{bmatrix} \quad (12)$$

where ρ represents the fluid density, g the gravitational acceleration, ∇ the displaced fluid volume and m the mass of the vehicle. Now, if we consider that $W = mg$ and $B = \rho g \nabla$ and using the *zyx*-convention for navigation and control application (Fossen, 2002), then the transformation matrix $J_1(\eta_2) = R_{z,\psi} R_{y,\theta} R_{x,\phi}$ is applied in order to obtain the weight and buoyancy forces with respect to the body-fixed frame:

$$F_B = J_1(\eta_2)^{-1} f_B F_W = J_1(\eta_2)^{-1} f_W \quad (13)$$

consequently,

$$F_B = \begin{bmatrix} Bsin(\theta) \\ -Bcos(\theta)sin(\phi) \\ -Bcos(\theta)cos(\phi) \end{bmatrix} F_W = \begin{bmatrix} -Wsin(\theta) \\ Wcos(\theta)sin(\phi) \\ Wcos(\theta)cos(\phi) \end{bmatrix} \quad (14)$$

Thus, the restoring forces acting on the vehicle are $f_g = F_B + F_W$, which leads to

$$f_g = \begin{bmatrix} (B - W)sin(\theta) \\ (W - B)cos(\theta)sin(\phi) \\ (W - B)cos(\theta)cos(\phi) \end{bmatrix} \quad (15)$$

Please cite this article in press as: Campos, E., et al., A nonlinear controller based on saturation functions with variable parameters to stabilize an AUV, International Journal of Naval Architecture and Ocean Engineering (2018), https://doi.org/10.1016/j.ijnaoe.2018.04.002

The restoring moments can be described by the following equation:

$$m_g = r_w \times F_W + r_b \times F_B \tag{16}$$

where $r_w = [x_w, y_w, z_w]^T$ and $r_b = [x_b, y_b, z_b]^T$ represent the positions of the Center of Gravity (CG) and the Center of Buoyancy (CB) respectively. Based on the design of the vehicle and to reduce further analysis, the origin of the body-fixed frame is chosen in the center of gravity, which implies that $r_w = [0,0,0]^T$; while the center of buoyancy is $r_b = [0,0,-z_b]^T$. For practical purposes, the buoyancy force is greater than the weight, i.e., $W - B = -f_b$. Then, from Eqs. (15) and (16), one can deduce:

$$g(\eta) = \begin{bmatrix} f_g \\ m_g \end{bmatrix} = \begin{bmatrix} f_b sin(\theta) \\ -f_b cos(\theta) sin(\phi) \\ -f_b cos(\theta) cos(\phi) \\ -z_b B cos(\theta) sin(\phi) \\ -z_b B sin(\theta) \\ 0 \end{bmatrix} \tag{17}$$

2.4. Forces and torques generated by the thrusters

Fig. 2 illustrates the forces generated by the thrusters acting on the vehicle. They are described relative to the body-fixed frame, as:

$$\widehat{f_1} = \begin{bmatrix} 0 \\ 0 \\ f_1 \end{bmatrix}; \widehat{f_2} = \begin{bmatrix} 0 \\ 0 \\ f_2 \end{bmatrix}; \widehat{f_3} = \begin{bmatrix} f_3 \\ 0 \\ 0 \end{bmatrix}; \widehat{f_4} = \begin{bmatrix} f_4 \\ 0 \\ 0 \end{bmatrix}$$

$$\widehat{f_5} = \begin{bmatrix} f_5 \\ 0 \\ 0 \end{bmatrix}; \widehat{f_6} = \begin{bmatrix} f_6 \\ 0 \\ 0 \end{bmatrix}; \widehat{f_7} = \begin{bmatrix} 0 \\ 0 \\ f_7 \end{bmatrix}; \widehat{f_8} = \begin{bmatrix} 0 \\ 0 \\ f_8 \end{bmatrix}$$

Summarizing and using the notations of (The Society of Naval Arch, 1950), it follows that:

$$\tau_1 = \begin{bmatrix} \tau_X \\ \tau_Y \\ \tau_Z \end{bmatrix} = \begin{bmatrix} f_3 + f_4 + f_5 + f_6 \\ 0 \\ f_1 + f_2 + f_7 + f_8 \end{bmatrix} \tag{18}$$

choose an the body-fixed torques generated by the above forces, are defined as:

$$\tau_2 = \sum_{i=1}^{6} l_i \times \widehat{f_i} \tag{19}$$

where $l_i = (l_{ix}, l_{iy}, l_{iz})$ is the position vector of the force $\widehat{f_i}$ $\forall$ $i = 1,..,$ 8, with respect to the body-fixed reference frame. The torques generated by the thrusters are described as:

$$\tau_2 = \begin{bmatrix} \tau_K \\ \tau_M \\ \tau_N \end{bmatrix} = \begin{bmatrix} l_{1y} f_1 - l_{1y} f_2 + l_{7y} f_7 - l_{7y} f_8 \\ l_{1x}(f_1 + f_2) - l_{7x}(f_7 + f_8) \\ l_{3y}(f_3 - f_5) + l_{4y}(f_4 - f_6) \end{bmatrix} \tag{20}$$

Given that we have connected two thrusters to the same driver, to reduce the cost of the underwater vehicle, then $f_1 = f_2, f_3 = f_4$, $f_5 = f_6$ and $f_7 = f_8$, as consequence:

$$\tau = \begin{bmatrix} 2f_3 + 2f_5 \\ 0 \\ 2f_1 + 2f_7 \\ 0 \\ 2l_{1x} f_1 - 2l_{7x} f_7 \\ (f_3 - f_5)(l_{3y} + l_{4y}) \end{bmatrix} \tag{21}$$

Remark 1. From *equation (21) we can observe that the vector of control input has 2 zeros, then the system has a lower number of input controls than degrees of freedom. Consequently, we have an underactuated system.*

2.5. Design considerations

To build of the *LIRMIA*2, we have considered the mathematical model to take advantage of the moments produced by the location of the gravity and buoyancy centers. Then, from Eq. (1) we can observe that if the gravity center is located in the origin $(0,0,0)$ of the body-fixed frame and the buoyancy center is located in $(0,0,-zb)$; we obtain the following conditions:

$$\left(I_x + K_{\dot{p}}\right)\dot{p} + D_\phi p = z_b B C_\theta S_\phi \quad \rightarrow \phi \approx 0 \tag{22}$$

$$\left(I_y + M_{\dot{q}}\right)\dot{q} + D_\theta q = Z_b B S_\theta \quad \rightarrow \theta \approx 0 \tag{23}$$

Notice that the moments are independent of the forces generated by the thrusters. In other words, we can assume that the angular position $\theta = \phi = 0$ during all the experiments without a control input. The other advantage is less energy consumption.

3. Proposed control strategy

In the above section, we described the vectors and the matrices that we estimated and measured to know the parameters of the mathematical model. However, uncertainty exists in estimating the parameters. Consequently, we propose a robustness control strategy for the set-point regulation and the trajectory tracking control take the uncertainty into account in the parameters of the system.

Let $u(t)$ be a PD controller whose expression is given by:

$$u(t) = k_1 e(t) + k_2 \frac{de(t)}{dt} \tag{24}$$

where $e(t) = r(t) - y(t)$ is the tracking error, $r(t)$ represents the reference, $y(t)$ is the measured output, k_1 and k_2 are the proportional and derivative feedback gains. From (24) we can observe that: if $e(t) \rightarrow \infty$ then $u(t) \rightarrow \infty$. This could lead to oscillations in the system or damage the actuators. A common practice is to propose some saturation function, as given below, would address these problems.

3.1. A nonlinear PD controller based on saturation functions

Let $\sigma_{\overline{b_i}}(k_i h_i)$ be a saturation function for $i = 1,2$, with $\overline{b_i}$ and k_i constant and positive definite, defined by the following equation:

$$\sigma_{\overline{b_i}}(k_i h_i) = \begin{cases} \overline{b_i} & if \quad k_i h_i > \overline{b_i} \\ k_i h_i & if \quad \left|k_i h_i\right| \leq \overline{b_i} \\ -\overline{b_i} & if \quad k_i h_i < -\overline{b_i} \end{cases} \tag{25}$$

where k_i is a gain, the parameter $\overline{b_i}$ is the value choose in order to limit the values of any function represented by h_i, in this case h_1 and h_2 represent de error and its derivative respectively.

To improve the performance of the closed-loop system and to avoid damage to the actuators, the controller given by Eq. (24) could be modified by using the above saturation functions in each term, leading to the following:

Please cite this article in press as: Campos, E., et al., A nonlinear controller based on saturation functions with variable parameters to stabilize an AUV, International Journal of Naval Architecture and Ocean Engineering (2018), https://doi.org/10.1016/j.ijnaoe.2018.04.002

$$U(t) = \sigma_{\overline{b_1}}[k_1 e(t)] + \sigma_{\overline{b_2}}\left[k_2 \frac{de(t)}{dt}\right] \tag{26}$$

Now, equation (26) can be rewritten in a compact form as:

$$U(t) = \sum_{i=1}^{2} u_i \tag{27}$$

where $u_i = \sigma_{\overline{b_i}}(k_i h_i)$ for $i = 1, 2$; represents the saturation of the proportional and derivative control action respectively. By applying equation (25) we can rewritten u_i as:

$$u_i = \begin{cases} sign(h_i)\overline{b_i} & if \quad \left|k_i h_i\right| > \overline{b_i} \\ k_i h_i & if \quad \left|k_i h_i\right| \leq \overline{b_i} \end{cases} \tag{28}$$

To introduce a modification of saturations (28), let us consider the point of h_i where $\left|u_i\right| = \overline{b_i}$, this is:

$$\left|u_i\right| = \left|k_i h_i\right| = \overline{b_i} \quad \Rightarrow \quad \left|h_i\right| = \overline{b_i} \Big/ k_i \tag{29}$$

then, we define

$$d_i := \overline{b_i} \Big/ k_i \tag{30}$$

as consequence, we have that:

$$u_i = sign(h_i)\overline{b_i} \quad \forall \quad |h_i| > d_i \tag{31}$$

According to Eqs. (30) and (31), we can express (28) as follows:

$$u_i = \begin{cases} sign(h_i)\overline{b_i} & if \quad |h_i| > d_i \\ \overline{b_i} d_i^{-1} h_i & if \quad |h_i| \leq d_i \end{cases} \tag{32}$$

where the tuning parameters of the controller are b_i and d_i, $\forall\ i = 1, 2$. To express Eq. (32) in terms of h_i, when $|h_i| > d_i$, we consider that:

$$sign(h_i)\overline{b_i} = h_i sign(h_i)\overline{b_i} h_i^{-1} \tag{33}$$

then

$$sign(h_i)\overline{b_i} = \left|h_i\right|\overline{b_i} h_i^{-1} \tag{34}$$

and considering that $\left|h_i\right| h_i^{-1} = \left|h_i\right|^{-1} h_i$, then Eq. (32) can be rewritten as:

$$u_i = \begin{cases} \overline{b_i}\left|h_i\right|^{-1} h_i & if \quad |h_i| > d_i \\ \overline{b_i} d_i^{-1} h_i & if \quad |h_i| \leq d_i \end{cases} \tag{35}$$

Finally, the law control defined by Eq. (26) can be represent as:

$$U(t) = u_1 + u_2 = k_p(e)e(t) + k_d(\dot{e})\dot{e}(t) \tag{36}$$

with

$$k_p(e) = \begin{cases} \overline{b_1}\left|e(t)\right|^{-1} & if \quad |e(t)| > d_1 \\ \overline{b_1} d_1^{-1} & if \quad |e(t)| \leq d_1 \end{cases} \tag{37}$$

$$k_d(\dot{e}) = \begin{cases} \overline{b_2}\left|\dot{e}(t)\right|^{-1} & if \quad |\dot{e}(t)| > d_2 \\ \overline{b_2} d_2^{-1} & if \quad |\dot{e}(t)| \leq d_2 \end{cases} \tag{38}$$

The advantage of this controller is that maximum forces and torque are chosen by the parameters $\overline{b_1}$ and $\overline{b_2}$. Thus, we can ensure that actuators will not be damaged. However, in other cases it will be necessary for forces and torque to be slightly larger to correct the system error. It is for this reason that we propose that the constant saturation value $\overline{b_i}$, from Eq. (35), to change as follows:

$$\overline{b_i} = \begin{cases} b_i\left|h_i\right|^{\mu_i} & if \quad |h_i| > d_i \\ b_i\left|d_i\right|^{\mu_i} & if \quad |h_i| \leq d_i \end{cases} \\ \forall i = 1, 2 \text{ and } \mu_i \in [0, 1] \tag{39}$$

Then, introducing Eq. (39) into Eq. (35) we obtain:

$$u_i = \begin{cases} b_i\left|h_i\right|^{\mu_i}\left|h_i\right|^{-1} h_i & if \quad |h_i| > d_i \\ b_i\left|d_i\right|^{\mu_i} d_i^{-1} h_i & if \quad |h_i| \leq d_i \end{cases} \\ \forall i = 1, 2 \text{ and } \mu_i \in [0, 1] \tag{40}$$

Consequently, from Eq. (40) we obtain a nonlinear PD controller as follows:

$$U(t) = u_1 + u_2 = k_p(e)e(t) + k_d(\dot{e})\dot{e}(t) \tag{41}$$

with

$$k_p(e) = \begin{cases} b_1\left|e(t)\right|^{(\mu_1 - 1)} & if \quad |e(t)| > d_1 \\ b_1 d_1^{(\mu_1 - 1)} & if \quad |e(t)| \leq d_1 \end{cases} \tag{42}$$

$$k_d(\dot{e}) = \begin{cases} b_2\left|\dot{e}(t)\right|^{(\mu_2 - 1)} & if \quad |\dot{e}(t)| > d_2 \\ b_2 d_2^{(\mu_2 - 1)} & if \quad |\dot{e}(t)| \leq d_2 \end{cases} \tag{43}$$

$\forall \mu_1, \mu_2 \in [0, 1]$.

Notice that the controller obtained in Eq. (41) is a PD controller with variable gains. To show the behavior of the variable gains given by Eqs. (42) and (43), we have plotted an example for different values of the parameter μ_i, with $d_i = 5$ and $b_i = 100$ in Fig. 3.

Remark 2. *The proposed nonlinear PD controller can be degenerated into the classical PD controller if $\mu_p = \mu_d = 1$, as is depicted in Fig. 3. On the other hand, if $\mu_p = \mu_d = 0$, we obtain the case of a constant value for a saturation function. As a result, the input control is completely bounded when $|h_i| > d_i$. On the other hand, the classical PD and the saturation PD with Eq. (25) is a particular case of the proposed controller.*

Remark 3. *The values of the gains $k_p(e)$ and $k_d(\dot{e})$ are constant when $|e(t)| \leq d_1$ and $|\dot{e}(t)| \leq d_2$, as is depicted in Fig. 3. This region is called the linear region of the input control.*

3.2. Set-point regulation

In this section, we present a Nonlinear Proportional Derivative control with Gravitational/buoyancy compensation (NPDG) for the case of set-point regulation. Based on the controller (41) and the dynamic model (1), we propose this control law:

$$\tau = J^T(\eta)\left[K_p(e)e + K_d(\dot{e})\dot{e}\right] + g(\eta) \tag{44}$$

Please cite this article in press as: Campos, E., et al., A nonlinear controller based on saturation functions with variable parameters to stabilize an AUV, International Journal of Naval Architecture and Ocean Engineering (2018), https://doi.org/10.1016/j.ijnaoe.2018.04.002

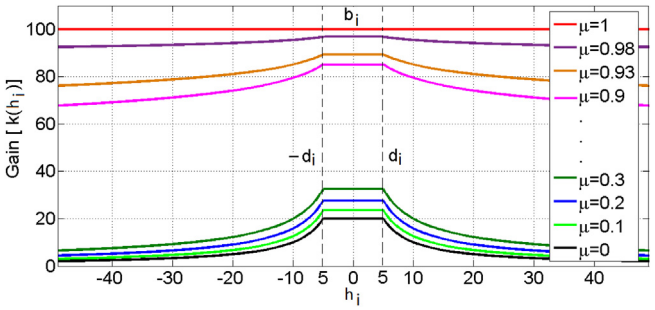

Fig. 3. Plot of a variable gain obtained by implementing a saturation function, described by Eq. (25), but changing the constant value of the parameter $\overline{b_i}$ for the function given by Eq. (39).

where the matrix $K_p(e)$ and $K_d(\dot{e})$ have the following structure:

$$K_p(e) = \begin{bmatrix} k_{p1}(e_1) & 0 & \dots & 0 \\ 0 & k_{p2}(e_2) & \dots & 0 \\ \vdots & \vdots & \ddots & \vdots \\ 0 & 0 & \dots & k_{pn}(e_n) \end{bmatrix} > 0 \tag{45}$$

$$K_d(\dot{e}) = \begin{bmatrix} k_{d1}\left(\dot{e_1}\right) & 0 & \dots & 0 \\ 0 & k_{d2}\left(\dot{e_2}\right) & \dots & 0 \\ \vdots & \vdots & \ddots & \vdots \\ 0 & 0 & \dots & k_{dn}\left(\dot{e_n}\right) \end{bmatrix} > 0 \tag{46}$$

with $k_{pj}(e_j)$ and $k_{dj}(\dot{e_j})$ defined by (42) and (43) respectively.

In Fig. 4 we show the diagram block of the closed-loop system with the NPDG controller.

3.2.1. Stability analysis of the closed-loop system

Since the controller will be a regulator and the error is $e = \eta_d - \eta$, then $\dot{e} = -\dot{\eta}$, as a consequence the control law given by Eq. (44) can be rewritten as:

$$\tau = J^T(\eta)\left[K_p(e)e - K_d(\dot{e})\dot{\eta}\right] + g(\eta) \tag{47}$$

Now assuming that $w_e = 0$, and introducing Eq. (47) into (1), the closed-loop system is:

$$M\dot{\nu} + C(\nu)\nu + D(\nu)\nu = J^T(\eta)\left[K_p(e)e - K_d(\dot{e})\dot{\eta}\right] \tag{48}$$

and according to Eq. (2), we obtain

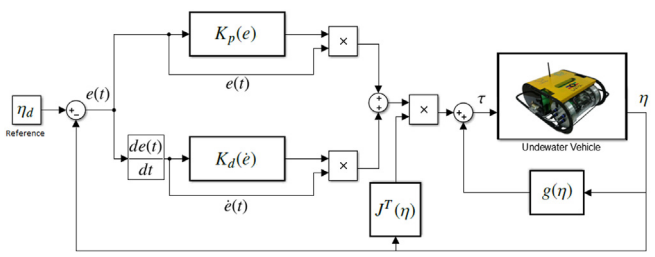

Fig. 4. In this diagram we show the closed-loop system with the proposed control strategy for the case of set-point regulation which is described by Eq. (44). Notice that the blocks $K_p(e)$ and $K_d(\dot{e})$ represent the variable gains which are computed by Eqs. (42) and (43) respectively. Observe that for the nonlinear PD controller with gravity/buoyancy compensation we need to know only the gravity/buoyancy vector and the transformation matrix $J^T(\eta)$ given by equation (2).

$$M\dot{\nu} + C(\nu)\nu + D(\nu)\nu = J^T(\eta)\left[K_p(e)e - K_d(\dot{e})J(\eta)\nu\right] \tag{49}$$

Let us define $K_{dd}(\eta, \dot{e}) = J^T(\eta)K_d(\dot{e})J(\eta)$, then the previous equation can be rewritten as

$$M\dot{\nu} + C(\nu)\nu + D(\nu)\nu = J^T(\eta)K_p(e)e - K_{dd}(\eta, \dot{e})\nu \tag{50}$$

The closed-loop system given by Eq. (50) could be represent as:

$$\frac{d}{dt}\begin{bmatrix} e \\ \nu \end{bmatrix} = \begin{bmatrix} -J(\eta)\nu \\ M^{-1}\left[J^T(\eta)K_p(e)e - K_{dd}(\eta, \dot{e})\nu - C(\nu)\nu - D(\nu)\nu\right] \end{bmatrix} \tag{51}$$

Notice that the origin of the state space model is a unique equilibrium point. To do the stability analysis, we use the following Lyapunov function candidate:

$$V(e, \nu) = \frac{1}{2}\nu^T M\nu + \int_0^e \xi^T K_p(\xi)d\xi \tag{52}$$

and assume that class K functions $\alpha_j(|e_j|)$ exist, such that:

$$e_j k_{pj}(e_j) \geq \alpha_j(|e_j|) \tag{53}$$

with

$$\alpha_j(|e_j|) = \begin{cases} \dfrac{b_\alpha |e_j|^{\mu_1} e_j}{a + |e_j|} & \text{if} \quad |e_j| > d_\alpha \\ \dfrac{b_\alpha d_\alpha^{\mu_1} e_j}{a + d_\alpha} & \text{if} \quad |e_j| \leq d_\alpha \end{cases} \tag{54}$$

where $b_1 > b_\alpha$, $a > 0$ and $d_1 < d_\alpha$. Then, according to *Lemma* 2 from (Kelly and Carelli, 1996)

$$\int_0^e \xi^T K_p(\xi)d\xi > 0 \forall e \neq 0 \in R^n \tag{55}$$

and

$$\int_0^e \xi^T K_p(\xi)d\xi \to \infty as ||e|| \to \infty \tag{56}$$

where

$$\int_0^e \xi^T K_p(\xi)d\xi = \int_0^{e_1} \xi_1 k_{p1}(\xi_1)d\xi_1 + \dots + \int_0^{e_n} \xi_n k_{pn}(\xi_n)d\xi_n.$$

Therefore $V(e, \nu)$ is a globally positive definite and radially unbounded function. The time derivative of the Lyapunov function candidate is:

$$\dot{V}(e, \nu) = \nu^T M\dot{\nu} - e^T K_p(e)J(\eta)\nu \tag{57}$$

By substituting the closed-loop Eq. (50) into (57) we obtain:

$$\begin{aligned} \dot{V}(e, \nu) = {} & \nu^T J^T(\eta)K_p(e)e - \nu^T K_{dd}(\eta, \dot{e})\nu - \\ & \nu^T C(\nu)\nu - \nu^T D(\nu)\nu - e^T K_p(e)J(\eta)\nu \end{aligned} \tag{58}$$

since $K_p(e) = K_p^T(e)$ and $C(\nu) = -C(\nu)^T$, Eq. (58) becomes:

Please cite this article in press as: Campos, E., et al., A nonlinear controller based on saturation functions with variable parameters to stabilize an AUV, International Journal of Naval Architecture and Ocean Engineering (2018), https://doi.org/10.1016/j.ijnaoe.2018.04.002

$$\dot{V}(e,\nu) = -\nu^T[K_{dd}(\eta,\dot{e}) + D(\nu)]\nu \tag{59}$$

Remember that $K_d = K_d^T > 0$, therefore $K_{dd} = K_{dd}^T > 0$, and assuming that $D(\nu) > 0$, then we obtain $\dot{V}(e,\nu)$ which is a globally negative semidefinite function. Therefore, we conclude stability of the equilibrium point. In order to prove asymptotic stability, we apply the Krasovskii-LaSalle's theorem:

$$\Omega = \left[\begin{bmatrix} e \\ \nu \end{bmatrix} : \dot{V}(e,\nu) = 0\right] = \left[\begin{bmatrix} e \\ \nu \end{bmatrix} = \begin{bmatrix} e \\ 0 \end{bmatrix} \in \mathbb{R}^{2n}\right] \tag{60}$$

Introducing $\nu = 0$ and $\dot{\nu} = 0$ into Eq. (50) we have $e = 0$. Therefore, we conclude that equilibrium point is globally asymptotically stable.

3.3. Trajectory tracking control

Based on Eq. (2) we obtain the following kinematic transformations (more details see (Fossen, 2002))

$$\ddot{\eta} = J(\eta)\dot{\nu} + \dot{J}(\eta)\nu \Rightarrow \dot{\nu} = J^{-1}(\eta)\left[\ddot{\eta} - \dot{J}(\eta)J^{-1}(\eta)\dot{\eta}\right]$$

applying the previous transformations to model (1), we have:

$$\begin{aligned} M_\eta(\eta) &= J^{-T}(\eta)MJ^{-1}(\eta) \\ C_\eta(\nu,\eta) &= J^{-T}(\eta)\left[C(\nu) - MJ^{-1}(\eta)\dot{J}(\eta)\right]J^{-1}(\eta) \\ D_\eta(\nu,\eta) &= J^{-T}(\eta)D(\nu)J^{-1}(\eta) \\ g_\eta(\eta) &= J^{-T}(\eta)g(\eta) \\ \tau_\eta(\eta) &= J^{-T}(\eta)\tau \end{aligned}$$

Consequently, the mathematical model given by (1) with respect to the inertial frame is:

$$M_\eta(\eta)\ddot{\eta} + C_\eta(\nu,\eta)\dot{\eta} + D_\eta(\nu,\eta)\dot{\eta} + g_\eta(\eta) = J^{-T}(\eta)\tau \tag{61}$$

Then, for the case of trajectory tracking control, we propose the follows Nonlinear PD + controller (NPD+):

$$\begin{aligned} \tau = J^T(\eta)\Big[&M_\eta(\eta)\ddot{\eta}_d + C_\eta(\nu,\eta)\dot{\eta}_d + D_\eta(\nu,\eta)\dot{\eta}_d \\ &+ g_\eta(\eta) + K_p(e)e + K_d(\dot{e})\dot{e}\Big] \end{aligned} \tag{62}$$

In Fig. 5, we show the diagram block of the closed-loop system with the NPD + controller.

3.3.1. Stability analysis of the closed-loop system

Introducing the above controller into Eq. (61), the closed-loop system is:

$$M_\eta(\eta)\ddot{e} = -C_\eta(\nu,\eta)\dot{e} - D_\eta(\nu,\eta)\dot{e} - K_p(e)e - K_d(\dot{e})\dot{e} \tag{63}$$

Eq. (63) can also be written as:

$$\frac{d}{dt}\begin{bmatrix} e \\ \dot{e} \end{bmatrix} = \begin{bmatrix} \dot{e} \\ -M_\eta(\eta)^{-1}\left[\left[C_\eta(\nu,\eta) + D_\eta(\nu,\eta) + K_d(\dot{e})\right]\dot{e} + K_p(e)e\right] \end{bmatrix} \tag{64}$$

The stability analysis is similar that previous section, but in this case the Lyapunov function candidate is:

$$V(e,\dot{e}) = \frac{1}{2}\dot{e}^T M_\eta(\eta)\dot{e} + \int_0^e \xi^T K_p(\xi)d\xi \tag{65}$$

According to arguments used in proof of the previous section, we conclude that $V(e,\dot{e})$ is a globally positive definite and radially

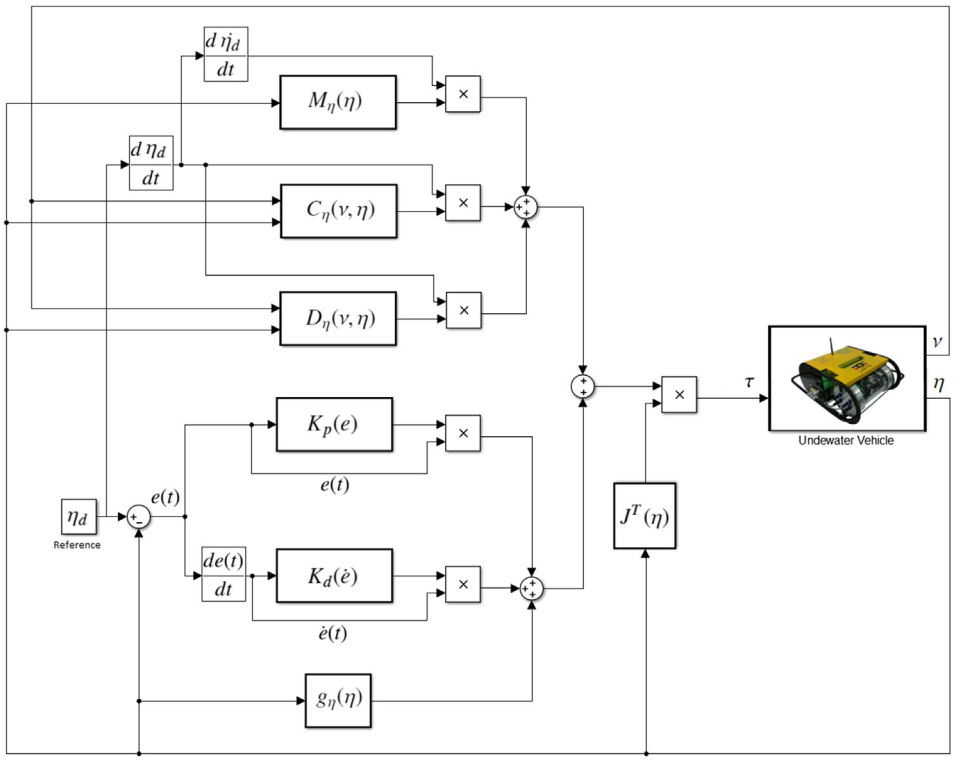

Fig. 5. In this diagram we show the closed-loop system with the proposed control strategy for the case of trajectory tracking control which is described by Eq. (62). Notice that in this case we need to know the mathematical model of the underwater vehicle given by Eq. (61) in order to compute the signal of the nonlinear PD + controller; however the variable gains are computing by the same equations that we have used for the NPDG controller.

Please cite this article in press as: Campos, E., et al., A nonlinear controller based on saturation functions with variable parameters to stabilize an AUV, International Journal of Naval Architecture and Ocean Engineering (2018), https://doi.org/10.1016/j.ijnaoe.2018.04.002

unbounded function. The time derivative of this Lyapunov function candidate is:

$$\dot{V}(e,\dot{e}) = \dot{e}^T M_\eta(\eta)\ddot{e} + \frac{1}{2}\dot{e}^T \dot{M}_\eta(\eta)\dot{e} + e^T K_p(e)\dot{e} \tag{66}$$

Now, introducing Eq. (63) into (66) and assuming that $\dot{M}_\eta = 0$, and $C_\eta(\nu,\eta)$ is skew symmetric, then:

$$\dot{V}(e,\dot{e}) = -\dot{e}^T\left[D_\eta(\nu,\eta) + K_d(\dot{e})\right]\dot{e} \tag{67}$$

assuming that $D_\eta(\nu,\eta) > 0$ and remember that $K_d(\dot{e}) > 0$ and symmetric matrix, then we obtain $\dot{V}(e,\dot{e})$ is a globally negative semidefinite function, and therefore we conclude stability of the equilibrium point. In order to prove asymptotic stability we apply the Krasovskii-LaSalle's theorem, then:

$$\Omega = \left[\begin{bmatrix} e \\ \dot{e} \end{bmatrix} : \dot{V}(e,\dot{e}) = 0\right] = \left[\begin{bmatrix} e \\ \dot{e} \end{bmatrix} = \begin{bmatrix} e \\ 0 \end{bmatrix} \in \mathbb{R}^{2n}\right] \tag{68}$$

Introducing $\dot{e} = 0$ and $\ddot{e} = 0$ into Eq. (63) we have $e = 0$, therefore the unique invariant is the origin. As a consequence we conclude that equilibrium point is globally asymptotically stable.

4. Real-time experiments

Fig. 6 shows the prototype that we have used in order to test our control strategies in real-time. The embedded system of *LIRMIA*2 consists in an embedded computer with an Intel Atom Z550 2 GHz CPU and a 1 GB DDR2-533 RAM memory. This embedded system also includes an inertial measurement unit (UM6 Orientation Sensor, CH Robotics), a Logitech webcam Pro 9000, and a pressure sensor Breakout-MS5803-05BA. The computer's operating system is Windows XP embedded. Using Visual C++, the computer processes the data from the sensors and sends the control inputs to the actuators. The weight and the buoyancy force of the vehicle are approximately 186.3*N* and 191.2*N*, respectively.

The main goal of the experiments is to test the advantage of the proposed controllers in real applications; then, in order to show the behavior of the closed-loop system with the proposed controllers we have implemented these only for the depth control problem in two cases:

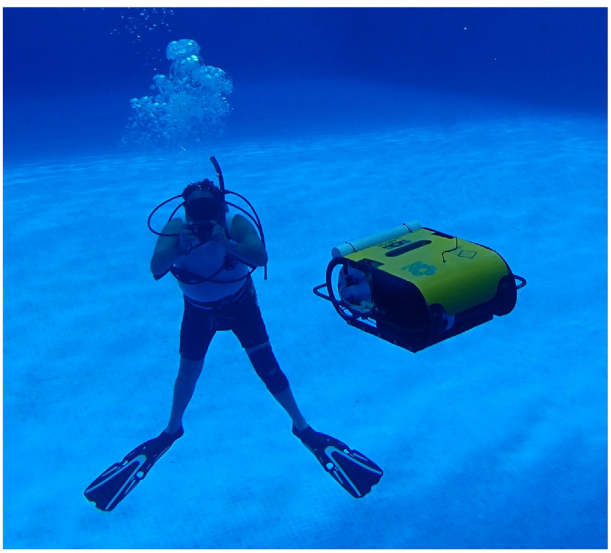

Fig. 6. *LIRMIA*2 prototype.

- CASE 1. Set-point regulation
- CASE 2. Trajectory tracking control

During this experiments we assume that $\phi = \theta = 0$ given the design conditions of the underwater vehicle *LIRMIA*2, and the θ will be close to zero since the lateral thrusters are turn off and the position about the axes x_I and y_I are also close to zero during all the experiments.

The control algorithm for all the proposed experiments was embedded in C++ programming and the pseudocode is presented in Table 2. Notice that the delay of the step 5 is in order to do all the experiments with the same initial conditions. The time to finish the experiments was chosen considering the performance of the closed-loop system.

4.1. Experimental results for set-point regulation

Taking into account the controller given by Eq. (44), then for the case of set-point regulation we have two scenarios. In the first one we consider $\mu_1 = \mu_2 = 1$, consequently we have a PD controller with gravitational/buoyancy compensation and the second scenario is when μ_1 and μ_2 are different to one, as consequence we obtain a nonlinear PD controller with gravitational/buoyancy compensation. Notice that in remark1 we have said: "If $\mu_1 = \mu_2 = 1$, then we have the case of a classical PD controller". These scenarios are chosen in order to show the advantage of implementing a saturation function with variable parameters, as we have described in the previous section. Then the scenarios are:

- CASE 1A: Considering that $\mu_1 = \mu_2 = 1$, then the controller given by Eq. (44) is a PD controller with Gravitational and buoyancy compensation (PDG).
- CASE 1B: Considering that μ_1 and μ_2 are different to one, then the controller given by Eq. (44) is a Nonlinear PD controller with Gravitational and buoyancy compensation (NPDG).

Notice that both cases are describe by Eq. (44), but with different gains values. The tuning of the both cases was done based on the experiments results taking into account the system performance,

Table 2
Embedded algorithm.

Embedded algorithm for the depth control of the *LIRMIA*2
1.- **Initiation**: choose the control problem
CASE 1: Set-point regulation, this is:
$\tau = J^T(\eta)[K_p(e)e + K_d(\dot{e})\dot{e}] + g(\eta)$
CASE 1A: Define $\mu_1 = \mu_2 = 1$
CASE 1B: Define μ_1 and μ_2 different to one
CASE 2: Trajectory traking control, this is:
$\tau = J^T(\eta)[M_\eta(\eta)\ddot{\eta_d} + C_\eta(\nu,\eta)\dot{\eta_d} + D_\eta(\nu,\eta)\dot{\eta_d} + g_\eta(\eta) + K_p(e)e + K_d(\dot{e})\dot{e}]$
CASE 2A: Define $\mu_1 = \mu_2 = 1$
CASE 2B: Define μ_1 and μ_2 different to one
2.- Define the gains parameters b_1, b_2, d_1 and d_2
3.- Calibration of the depth sensor
4.- Reset of the time = 0
5.- **Wait 10 s**
6.- Get the data from sensors (Depth and Attitude sensors)
7.- Compute the variable gains $K_p(e)$ and $K_d(\dot{e})$ with:
$k_p(e) = \begin{cases} b_1\lvert e(t)\rvert^{(\mu_1-1)} & if \quad \lvert e(t)\rvert > d_1 \\ b_1 d_1^{(\mu_1-1)} & if \quad \lvert e(t)\rvert \le d_1 \end{cases}$ $k_d(\dot{e}) = \begin{cases} b_2\lvert \dot{e}(t)\rvert^{(\mu_2-1)} & if \quad \lvert \dot{e}(t)\rvert > d_2 \\ b_2 d_2^{(\mu_2-1)} & if \quad \lvert \dot{e}(t)\rvert \le d_2 \end{cases}$ $\forall\, \mu_1, \mu_2 \in [0,1]$
8.- Compute the control input τ
9.- Send control signals to the thrusters
10.- Acquire and save data responses in a text file
11.- If time $<$ 300 s then **return to step 6**
12.- **END**

Please cite this article in press as: Campos, E., et al., A nonlinear controller based on saturation functions with variable parameters to stabilize an AUV, International Journal of Naval Architecture and Ocean Engineering (2018), https://doi.org/10.1016/j.ijnaoe.2018.04.002

Table 3
Gains values of the PDG controller.

$b_1 = 165$	$d_1 = 1$	$\mu_1 = 1$
$b_2 = 225$	$d_2 = 1$	$\mu_2 = 1$

Table 4
Gains values of the NPDG controller.

$b_1 = 104$	$d_1 = 0.003$	$\mu_1 = 0.9$
$b_2 = 200$	$d_2 = 0.007$	$\mu_2 = 0.95$

the time response without overshoot and considering the value of the Mean Square Error (*MSE*). After several experiments we obtain for the CASE 1A, the gains values which are shown in Table 3, while the gains values of the CASE 1B are shown in Table 4.

After doing the tuning task we have done two experiments for each case, the first we called the nominal case, it means that the vehicle has the same conditions that we have used for the tuning task. The second experiment was done after change the vehicle buoyancy in order to show the robustness of the NPDG controller when there is uncertainty in the parameters of the system. Observe that all the experiments start after 10 s in order to avoid the wave perturbations that we produce when we put the vehicle inside of the water and also notices that the maximum force τ_z produce by the thrusters is approximately 22 N, then the experiments are listed as follow:

- Experiment 1 (Exp_1): In this experiment the reference is $z_d = 1$ meter and the buoyancy force of the vehicle is approximately 191.2*N*.
- Experiment 2 (Exp_2): In this experiment the reference is $z_d = 1$ meter and the buoyancy force of the vehicle is approximately 193*N*.

The experimental results of the CASE 1A for the experiment 1 are shown in Fig. 7. In this Figure we can observe that the vehicle takes about 17 s to arrive to the reference depth, the gains $k_p(e)$ and $k_d(\dot{e})$ are constants and the computed MSE is 0.2077 m.

The experimental results of the CASE 1B for the experiment 1 are shown in Fig. 8. In this Figure we can observe that the vehicle takes about 18.5 s to arrive to the reference depth, the gains $k_p(e)$ and $k_d(\dot{e})$ are not constants and the computed MSE is 0.1995 m.

The experimental results of the CASE 1A for the experiment 2 are shown in Fig. 9. In this Figure we can observe that the vehicle never arrive to the reference depth, the gains $k_p(e)$ and $k_d(\dot{e})$ are constants and the computed MSE is 0.3102 m.

The experimental results of the CASE 1B for the experiment 2 are shown in Fig. 10. In this Figure we can observe that the vehicle takes about 19.5 s to arrive the reference depth, the gains $k_p(e)$ and $k_d(\dot{e})$ are not constants and the computed MSE is 0.2526 m.

Now, in Table 5 we show the computed mean square error for each experiment. Consequently we can conclude that the nonlinear PD controller with gravitational/buoyancy compensation (CASE 1B) has a better performance, from the practical point of view, in both experiments. On other words we can say that the proposed controller is robustness in the uncertainty of the parameters system. In addition, observe that the pitch angle (θ) is close to zero during all the experiments without input control due the design of the vehicle.

4.2. Experimental results for trajectory tracking control

Taking into account the controller given by Eq. (62), then we have also two scenarios for the trajectory tracking control. In the first one we consider $\mu_1 = \mu_2 = 1$, consequently we have a PD + controller and the second scenario is when μ_1 and μ_2 are different to one, as consequence we obtain a nonlinear PD + controller. Then these scenarios are:

- CASE 2A: Considering that $\mu_1 = \mu_2 = 1$, then the controller given by Eq. (62) is a PD + controller (PD+).
- CASE 2B: Considering that μ_1 and μ_2 are different to one, then the controller given by Eq. (62) is a Nonlinear PD + controller (NPD+).

For the experiments of trajectory tracking control the reference value z_d is a smooth trajectory function produce by a second order filter, then the tuning of the gains values was based on the experiments results taking into account the system performance, the

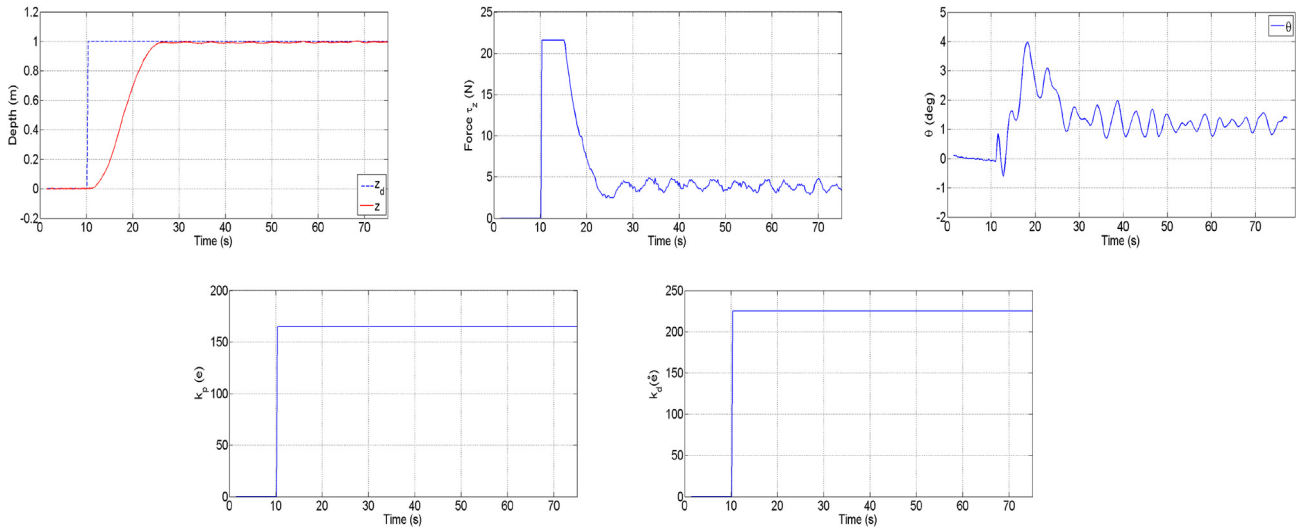

Fig. 7. Experimental results considering that $\mu_1 = \mu_2 = 1$, then the controller given by Eq. (44) is a PD controller with Gravitational and buoyancy compensation (PDG), with $z_d = 1$ meter and the buoyancy force of the vehicle is approximately 191.2*N*.

Please cite this article in press as: Campos, E., et al., A nonlinear controller based on saturation functions with variable parameters to stabilize an AUV, International Journal of Naval Architecture and Ocean Engineering (2018), https://doi.org/10.1016/j.ijnaoe.2018.04.002

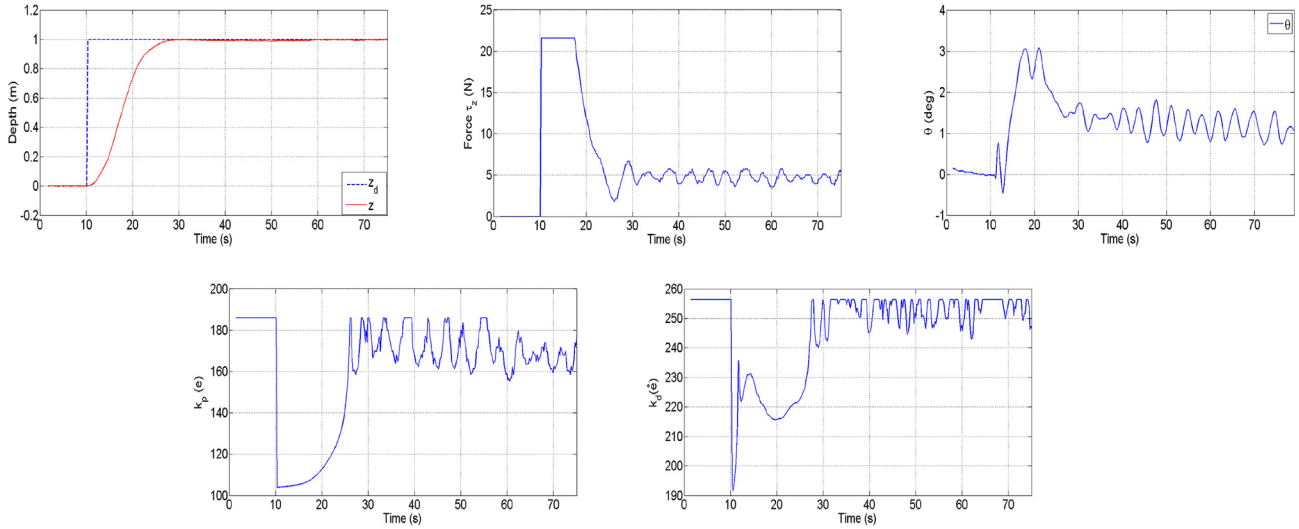

Fig. 8. Experimental results considering that μ_1 and μ_2 are different to one, then the controller given by Eq. (44) is a Nonlinear PD controller with gravitational and buoyancy compensation (NPDG), with $z_d = 1$ meter and the buoyancy force of the vehicle is approximately 191.2*N*.

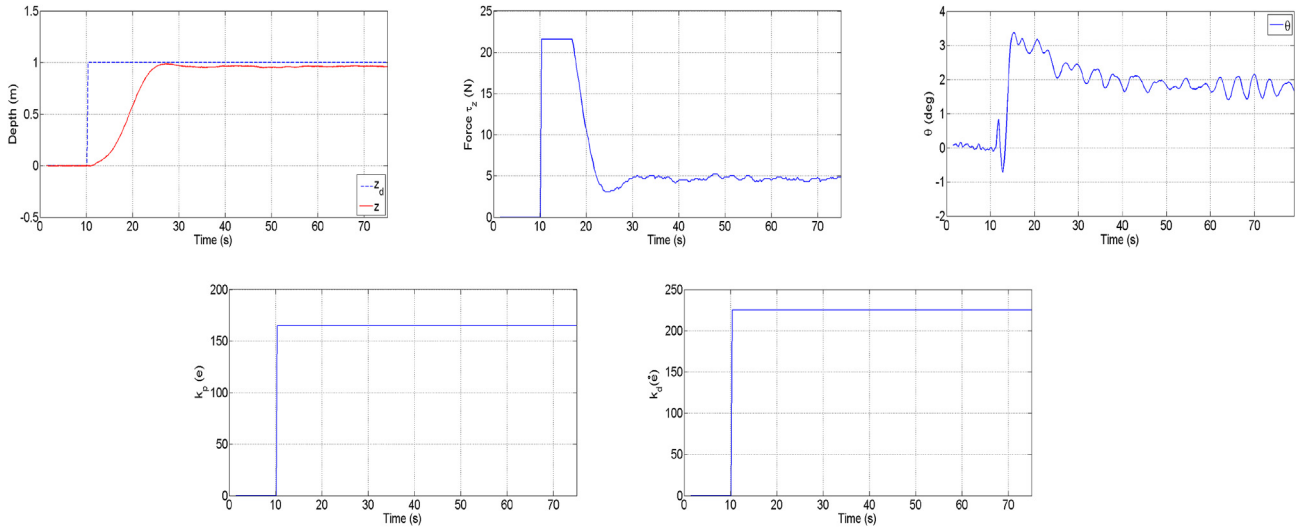

Fig. 9. Experimental results considering that $\mu_1 = \mu_2 = 1$, then the controller given by Eq. (44) is a PD controller with Gravitational and buoyancy compensation (PDG), with $z_d = 1$ meter and the buoyancy force of the vehicle is approximately 193*N*.

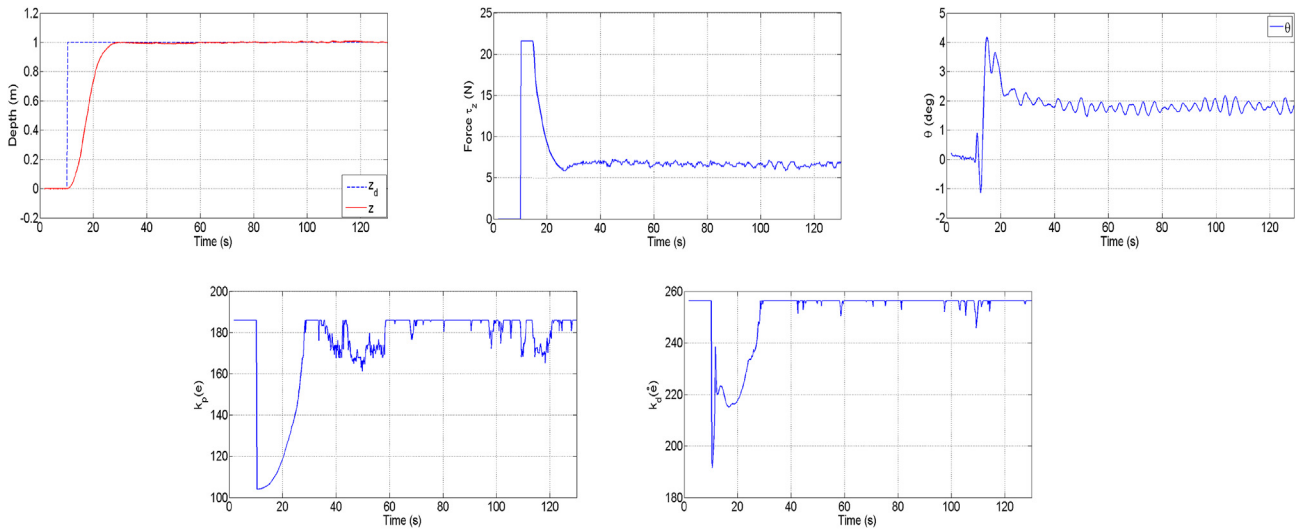

Fig. 10. Experimental results considering that μ_1 and μ_2 are different to one, then the controller given by Eq. (44) is a Nonlinear PD controller with Gravitational and buoyancy compensation (NPDG), with $z_d = 1$ meter and the buoyancy force of the vehicle is approximately 193*N*.

Please cite this article in press as: Campos, E., et al., A nonlinear controller based on saturation functions with variable parameters to stabilize an AUV, International Journal of Naval Architecture and Ocean Engineering (2018), https://doi.org/10.1016/j.ijnaoe.2018.04.002

Table 5
Mean square error for set-point regulation.

	Exp_1	Exp_2
Case 1A	0.2077	0.3102
Case 1B	0.1995	0.2526

Table 6
Gains of the PD + controller.

$b_1 = 165$	$d_1 = 1$	$\mu_1 = 1$
$b_2 = 225$	$d_2 = 1$	$\mu_2 = 1$

Table 7
Gains of the NPD + controller.

$b_1 = 165$	$d_1 = 0.025$	$\mu_1 = 0.75$
$b_2 = 225$	$d_2 = 0.05$	$\mu_2 = 0.85$

time response and the value of the MSE. After several experiments we obtain for the CASE 2A the gains values which are shown in Table 6, while the gains values of the CASE 2B are shown in Table 7.

After doing the tuning task we have done four experiments for each case with the following features:

- Experiment 1 (Exp_1): In this experiment the vehicle has the same conditions that we have used for the tuning task, it is weight = 186.3 N and buoyancy = 191.2 N.
- Experiment 2 (Exp_2): In this experiment we only change the vehicle weight, its weight = 188 N and the buoyancy = 191.2 N.
- Experiment 3 (Exp_3): In this experiment we only change the vehicle buoyancy, its weight = 186.3 N and the buoyancy = 193 N.
- Experiment 4 (Exp_4): In this experiment the vehicle has the same conditions of the experiment 1, but we have changed the trajectory reference.

The experimental results of the CASE 2A for the experiment 1 are shown in Fig. 11. In this Figure we can observe that the vehicle takes about 15 s to be close to the reference depth, the gains $k_p(e)$ and $k_d(\dot{e})$ are constants and the computed MSE is 0.0534 m.

The experimental results of the CASE 2B for the experiment 1 are shown in Fig. 12. In this Figure we can observe that the vehicle takes about 15 s to be close to the reference depth, the gains $k_p(e)$ and $k_d(\dot{e})$ are not constants and the computed MSE is 0.0508 m.

The experimental results of the CASE 2A for the experiment 2 are shown in Fig. 13. In this Figure we can observe that the vehicle takes about 16 s to be close to the reference depth, the gains $k_p(e)$ and $k_d(\dot{e})$ are constants and the computed MSE is 0.0966 m.

The experimental results of the CASE 2B for the experiment 2 are shown in Fig. 14. In this Figure we can observe that the vehicle takes about 14 s to be close to the reference depth, the gains $k_p(e)$ and $k_d(\dot{e})$ are not constants and the computed MSE is 0.0539 m.

The experimental results of the CASE 2A for the experiment 3 are shown in Fig. 15. In this Figure we can observe that the vehicle takes about 23 s to be close to the reference depth, the gains $k_p(e)$ and $k_d(\dot{e})$ are constants and the computed MSE is 0.0694 m.

The experimental results of the CASE 2B for the experiment 3 are shown in Fig. 16. In this Figure we can observe that the vehicle takes about 14 s to be close to the reference depth, the gains $k_p(e)$ and $k_d(\dot{e})$ are not constants and the computed MSE is 0.0535 m.

The experimental results of the CASE 2A for the experiment 4 are shown in Fig. 17. In this Figure we can observe that the vehicle takes about 16 s to be close to the reference depth, the gains $k_p(e)$ and $k_d(\dot{e})$ are constants and the computed MSE is 0.0960 m.

The experimental results of the CASE 2B for the experiment 4 are shown in Fig. 18. In this Figure we can observe that the vehicle takes about 16 s to be close to the reference depth, the gains $k_p(e)$ and $k_d(\dot{e})$ are not constants and the computed MSE is 0.0755 m.

From Table 8 we can say that the system performance is not affected significantly using the nonlinear PD + controller than using the PD + controller. Now, we can observe the advantage of the proposed controller in real applications and Finally it can be concluded that the proposed control strategy is robust to changes of parameters in the system. In addition observe that the pitch angle (θ) is close to zero during all the experiments even for the trajectory tracking control.

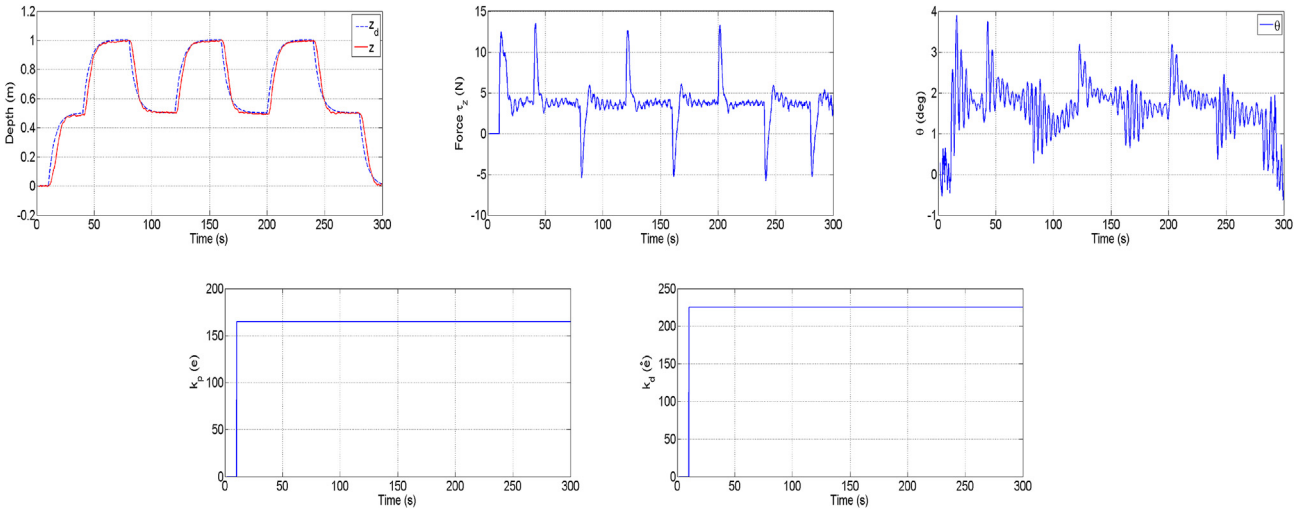

Fig. 11. Experimental results considering that $\mu_1 = \mu_2 = 1$, then the controller given by equation (62) is a PD + controller (PD+). In this experiments the vehicle has the same conditions that we have used for the tuning task, its weight = 186.3 N and buoyancy = 191.2 N.

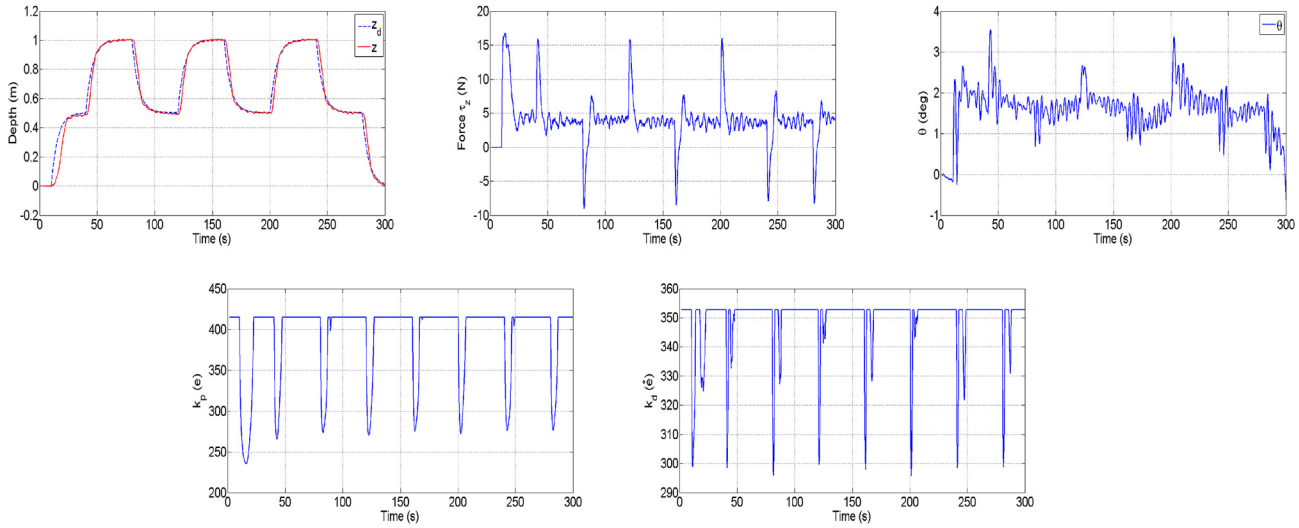

Fig. 12. Experimental results considering that μ_1 and μ_2 are different to one, then the controller given by equation (62) is a Nonlinear PD + controller (NPD+). In this experiments the vehicle has the same conditions that we have used for the tuning task, its weight = 186.3 N and buoyancy = 191.2 N.

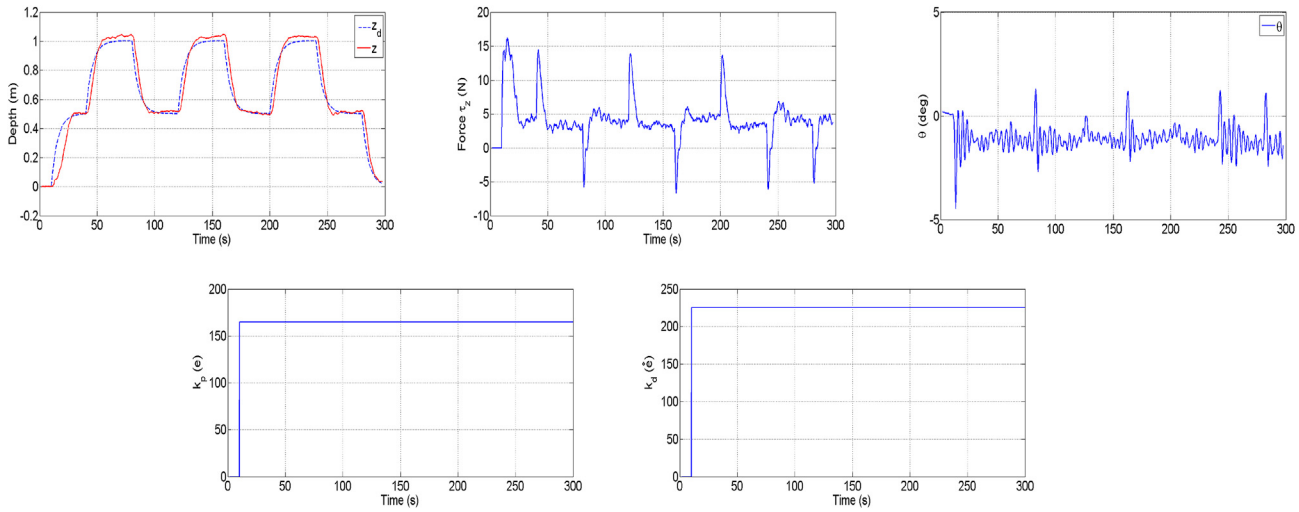

Fig. 13. Experimental results considering that $\mu_1 = \mu_2 = 1$, then the controller given by equation (62) is a PD + controller (PD+). In this experiment we only changed the vehicle weight, its weight = 188 N and buoyancy = 191.2 N.

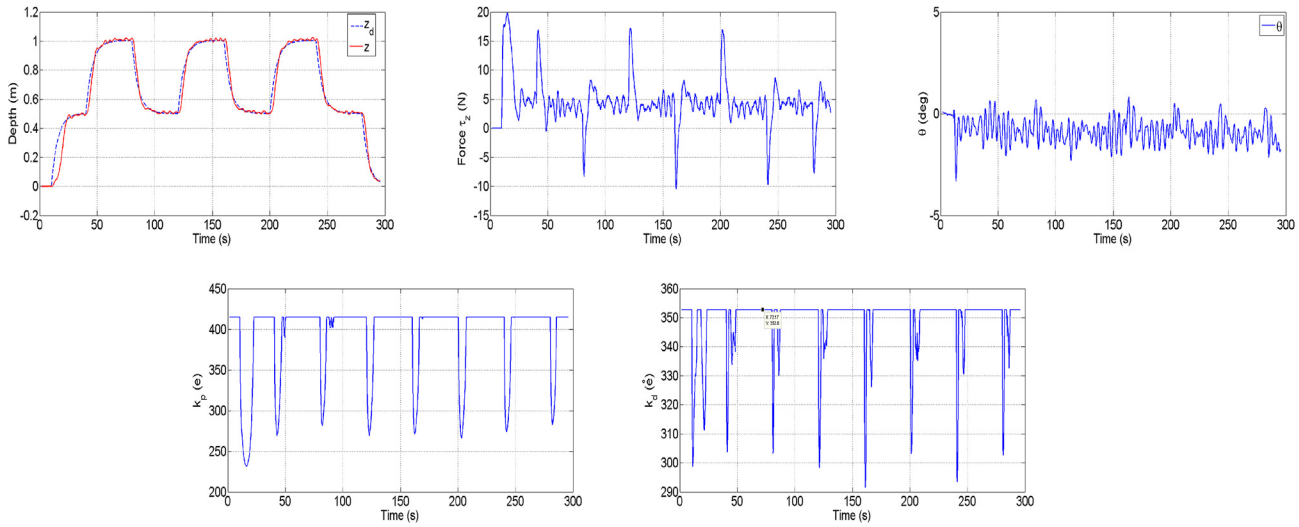

Fig. 14. Experimental results considering that μ_1 and μ_2 are different to one, then the controller given by equation (62) is a Nonlinear PD + controller (NPD+). In this experiment we only changed the vehicle weight, its weight = 188 N and buoyancy = 191.2 N.

Please cite this article in press as: Campos, E., et al., A nonlinear controller based on saturation functions with variable parameters to stabilize an AUV, International Journal of Naval Architecture and Ocean Engineering (2018), https://doi.org/10.1016/j.ijnaoe.2018.04.002

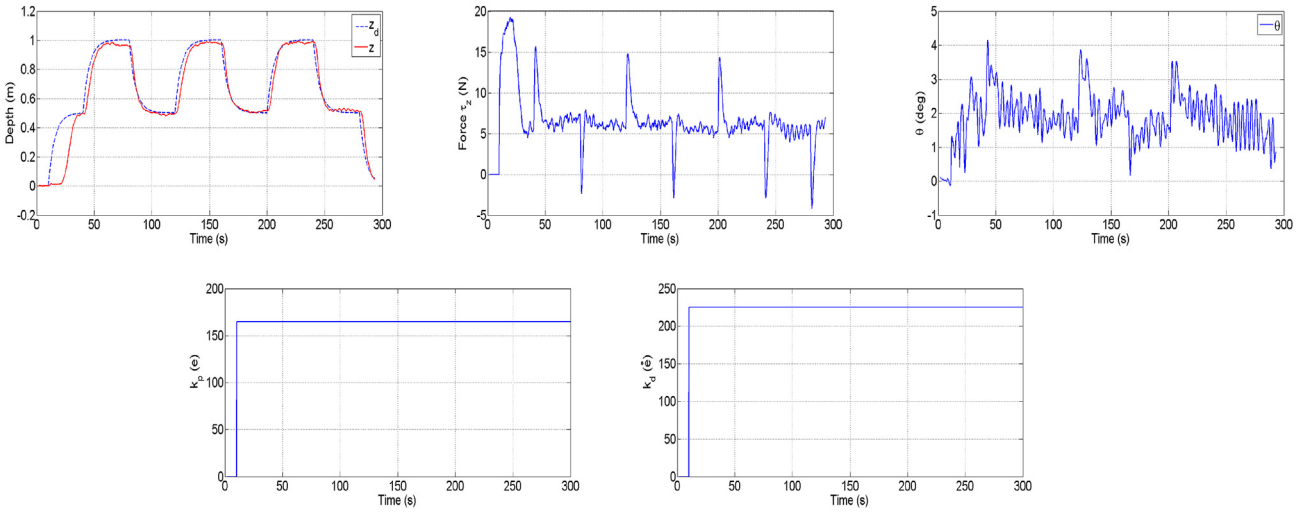

Fig. 15. Experimental results considering that $\mu_1 = \mu_2 = 1$, then the controller given by equation (62) is a PD + controller (PD+). In this experiments we only changed the vehicle buoyancy, its weight = 186.3 N and buoyancy = 193 N.

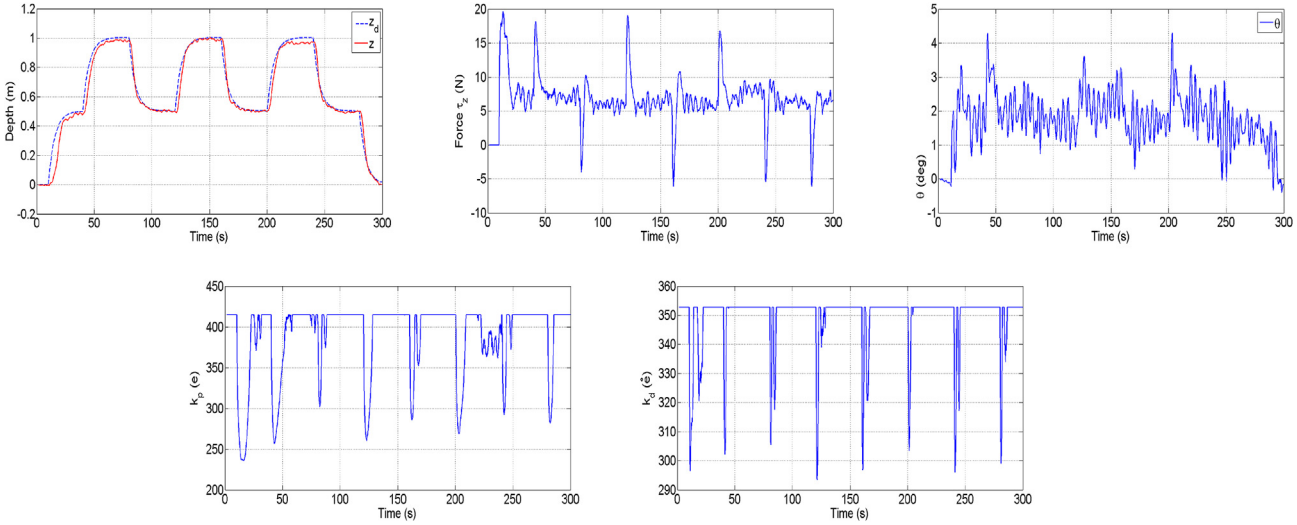

Fig. 16. Experimental results considering that μ_1 and μ_2 are different to one, then the controller given by equation (62) is a Nonlinear PD + controller (NPD+). In this experiments we only changed the vehicle buoyancy, its weight = 186.3 N and buoyancy = 193 N.

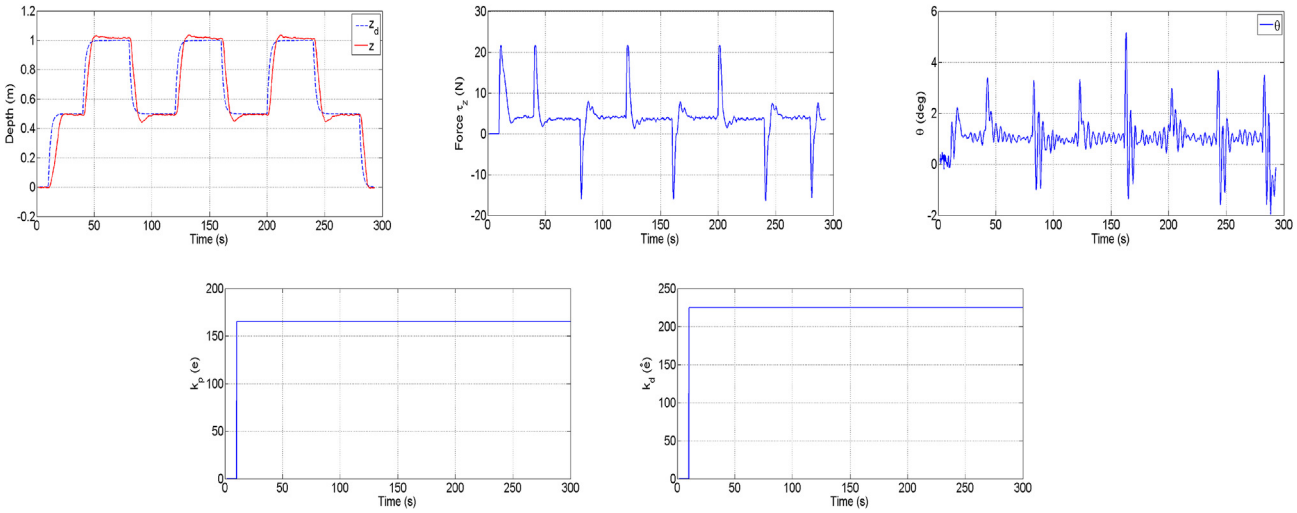

Fig. 17. Experimental results considering that $\mu_1 = \mu_2 = 1$, then the controller given by equation (62) is a PD + controller (PD+). In this experiment the vehicle has the same conditions than experiment 1, but we have changed the trajectory reference.

Please cite this article in press as: Campos, E., et al., A nonlinear controller based on saturation functions with variable parameters to stabilize an AUV, International Journal of Naval Architecture and Ocean Engineering (2018), https://doi.org/10.1016/j.ijnaoe.2018.04.002

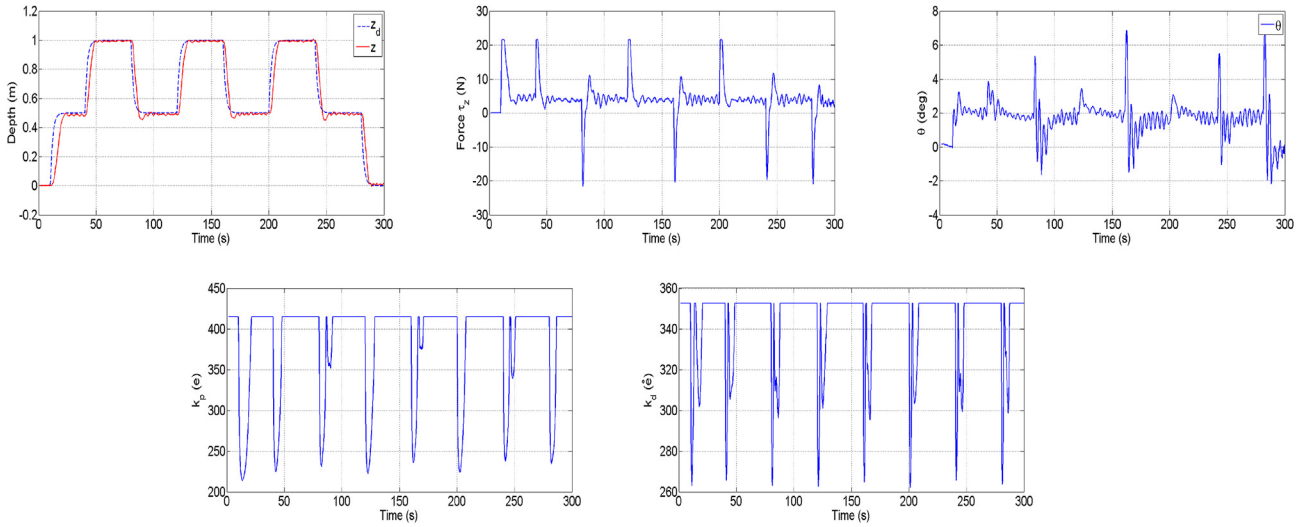

Fig. 18. Experimental results considering that μ_1 and μ_2 are different to one, then the controller given by equation (62) is a Nonlinear PD + controller (NPD+). In this experiment the vehicle has the same conditions than experiment 1, but we have changed the trajectory reference.

Table 8
Mean Square Error for trajectory tracking control.

	Exp_1	Exp_2	Exp_3	Exp_4
Case 2A	0.0534	0.0966	0.0694	0.0960
Case 2B	0.0508	0.0539	0.0535	0.0755

5. Conclusion and future work

The proposed NPDG and NPD + controllers for set-point regulation and trajectory tracking control, respectively, are robustness in the uncertainty of the parameters systems. We have proved that the equilibrium point of the closed-loop system with the proposed controllers is asymptotically stable using the Lyapunov arguments. The viability of the proposed NPDG and NPD + controllers were tested in real-time experiments, where we can notice that the advantage of implementing the saturation functions with variable parameters in a NPDG and NPD + controllers. In a next future, we will implement the integral part in order to improve the performance of the system. Experiments in presence of external disturbances will be soon conducted in natural environment.

References

Campos, E., Torres, I., et al., 2012. *Embedded system for controlling a mini underwater vehicle in autonomous hover mode* 1st IFAC Conference on Embedded Systems. Comput. Intell. Telematics Contr. 45, 266–271.
Fossen, Thor I., 1999. Guidance and Control of Ocean Vehicles. John Wiley and Sons.
Fossen, Thor I., 2002. Marine control Systems Guidance, Navigation, and Control of Shipd, Rigs and Underwater Vehicles Marine Cybernetics.
Fossen, Thor I., 2011. Handbook of Marine Craft Hydrodynamics and Motion Control. John Wiley.
Goldstein, H., Poole, C.P., Safko, J.L., 1983. Classical Mechanics Addison Wesley Series in Physics, second ed. Adison-Wesley.
Jung, Chul-Min, Paik, Bu-Geun, et al., 2017. Effects of the partially movable control fin with end plate of underwater vehicle. Int. J. Nav. Architect. Ocean. Eng. 9, 55–65.
Kawano, H., Ura, T., 2002. Fast reinforcement learning algorithm for motion planning of non-holonomic underwater vehicle disturbance. In: Int. Conference on Intelligent Robots and Systems IEEE/RSJ, vol. 1, pp. 903–908.
Kelly, R., Carelli, R., 1996. A class of nonlinear PD-type controller for robot manipulator. J. Field Robot. 13, 765–855.
L. Kleeman. *Advanced Sonar and odometry error Modeling for simultaneous Localization and map building* IEEE/RSJ International Conference on Intelligent Robots and Systems, vol. 1, pp. 699–704.
Lamb, H., 1932. Hydrodynamics. Cambridge University Press.
Maalouf, D., Tamanaja, I., et al., 2013. From PD to nonlinear adaptive Depth-Control of a tethered autonomous Underwater vehicle. In: 5th IFAC Symposium on System Structure and Control, vol. 46, pp. 743–748.
Marsden, J.E., 1974. Elementary Classical Analysis. W.H. Freeman and Company, San Francisco.
Newman, J.N., 1977. Marine Hydrodynamics. MIT Press, Cambridge.
Quidu, I., Jaulin, L., et al., 2012. Robust multitarget Tracking in forward looking sonar image Sequences using navigational data. IEEE J. Ocean. Eng. 37, 417–430.
Sanahuja, G., Castillo, P., Sanchez, A., 2009. Stabilization of n integrators in cascade with bounded input with experimental application to a VTOL laboratory system. Int. J. Robust Nonlinear Control 20, 1129–1139.
Stewart, A., Glegg, L., 2010. A passive sonar system Based on an autonomous underwater vehicle. IEEE J. Ocean. Eng. 26, 700–710.
The society of naval architects and marine engineers *Nomenclature for Treating the Motion of a submerged body Through a fluid.* Tech. Res. Bull., 1950 1–5.
Wallace, M., Bessa, et al., 2008. Depth control of remotely operated underwater vehicles using an adaptive fuzzy sliding mode controller. Robot. Autonom. Syst. 56, 670–677.
Shang, Weiwei, Cong, shuang, 2009. Nonlinear computed torque control for a high-speed planar parallel manipulator. Mechatron. Elsevier J. 19, 987–992.
Yang, Rui, Clement, Benoit, Mansour, Ali, Li, Ming, Wu, Nailong, 2015. Modeling of a complex-shaped underwater vehicle for robust control scheme. J. Intell. Rob. Syst. 80, 491–506.
Zhao, Li-Ye, Liu, Xian-Jun, et al., 2016. A pretreatment Method for the Velocity of DVL Based on the motion Constraint for the integrated SINS/DVL. Appl. Sci. 6, 79–86.

Please cite this article in press as: Campos, E., et al., A nonlinear controller based on saturation functions with variable parameters to stabilize an AUV, International Journal of Naval Architecture and Ocean Engineering (2018), https://doi.org/10.1016/j.ijnaoe.2018.04.002